

Initial Trajectory Assessment of the RAMSES Mission to (99942) Apophis

Andrea C. Morelli^{1†}, Alessandra Mannocchi^{1†},
Carmine Giordano^{1*}, Fabio Ferrari¹, Francesco Topputo¹

¹Department of Aerospace Science and Technology, Politecnico di
Milano, via La Masa, 34, Milan, 20156, Italy.

*Corresponding author(s). E-mail(s): carmine.giordano@polimi.it;
Contributing authors: andreacarlo.morelli@polimi.it;
alessandra.mannocchi@polimi.it; fabio1.ferrari@polimi.it;
francesco.topputo@polimi.it;

[†]These authors contributed equally to this work.

Abstract

(99942) Apophis is a potentially hazardous asteroid that will closely approach the Earth on April 13, 2029. Although the likelihood of an impact has been ruled out, this close encounter represents a unique opportunity for planetary science and defense. By investigating the physical and dynamical changes induced by this interaction, valuable insights into asteroid cohesion, strength, and internal structure can be obtained. In light of these circumstances, a fast mission to Apophis holds great scientific importance and potential for understanding potentially hazardous asteroids. To this aim, ESA proposed the mission RAMSES (Rapid Apophis Mission for SEcurity and Safety) to reach Apophis before its close encounter. In this context, the paper focuses on the reachability analysis of (99942) Apophis, examining thousands of trajectories departing from Earth and reaching the asteroid before the fly-by, using a low-thrust spacecraft. A two-layer approach combining direct sequential convex programming and an indirect method is employed for fast and reliable trajectory optimization. The results reveal multiple feasible launch windows and provide essential information for mission planning and system design.

Keywords: Apophis, Trajectory Design, Convex Optimization, Indirect Methods, RAMSES mission

1 Introduction

(99942) Apophis is a potentially hazardous asteroid with a diameter of about 370 metres that caused a brief period of concern in December 2004 when initial observations indicated a probability up to 2.7% that it would hit the Earth on April 13, 2029 (Chesley, 2005). Subsequent observations, however, improved predictions and ruled out the possibility of impact (Giorgini et al, 2008). Nevertheless, Apophis will pass within 31,000 km of Earth’s surface, closer than geosynchronous satellites (Sokolov et al, 2012).

While it is certain that Apophis will miss the Earth, the exact consequences on the asteroid itself remain uncertain (Zhang and Michel, 2020), with the main question lying in our limited knowledge of Apophis’ internal structure. As a matter of fact, the close encounter with the Earth will subject Apophis to significant tidal torques. Earth’s gravitational interactions with Apophis will likely modify its physical and dynamical properties, providing valuable insights into asteroid cohesion and strength (Souhay et al, 2014; Valvano et al, 2022). Depending on those, the asteroid could experience different outcomes, from measurable seismic waves and real-time surface disturbance (DeMartini et al, 2019), to local surface effects (Scheeres et al, 2005), up to the complete surface reshaping (Yu et al, 2014; Kim et al, 2023). For this reason, this encounter presents an unprecedented planetary defense and science opportunity, and a mission to Apophis has the potential to revolutionize our understanding of the internal structure of asteroids, which is crucial for effective planetary defense missions (Binzel et al, 2021).

As direct consequence of this celestial event, NASA has recently announced that Apophis will be the selected target of Osiris-REx extended mission (DellaGiustina et al, 2022). On the other hand, ESA proposed the mission RAMSES (Rapid Apophis Mission for SEcurity and Safety) having the aim to reach Apophis before the Earth close encounter¹. Its objective is to accompany the asteroid during the fly-by in order to determine the physical and dynamical changes induced by the interaction with the gravity of the Earth.

In the context of the RAMSES mission, the present work aims to scrutinize the reachability of the Apophis asteroid. Reachability analysis is an essential task in the preliminary assessment of asteroid missions (Wagner et al, 2015; Machuca et al, 2020; Topputo et al, 2021). In this work, all the possible trajectories departing from the Earth and reaching Apophis before the Earth fly-by are computed and their overall costs are estimated. The best suitable options are identified, and relevant figures that support the system design are evaluated. The variation of the required propellant mass with the departure date and Time of Flight (ToF) have to be produced, with thousands of trajectories to be computed. For this reason, a fast and reliable approach is necessary, in order to have the full envelope of the transfers to Apophis in a relatively small time. To this aim, a two-layer approach has been employed. It first exploits the flexibility of a sequential convex programming algorithm and then an indirect method, the latter guaranteeing the optimality of the solutions.

The paper is structured as follows. Section 2 presents an overview of the assumptions

¹<https://esastar-publication-ext.sso.esa.int/ESATenderActions/details/56945> (last accessed: July 7, 2023)

made on the mission and on the platform. Section 3 shows the approach used to fast solve the Apophis reachability problem, with details on the employed methodology. The results are presented in Section 4. Conclusions are drawn in Section 5.

2 Mission overview and assumptions

RAMSES is a small satellite mission that aims at the characterization of the dynamical and physical properties of asteroid Apophis before its close encounter with the Earth, on April 13, 2029, and their changes during the fly-by. Considering the Earth fly-by's close temporal proximity, the whole mission design and implementation is strictly driven by time constraints. As a matter of fact, in order to properly map the pre-fly-by characteristics of Apophis, the spacecraft shall reach the asteroid at least 2 months before the encounter. On the other hand, a time frame of at least 3 years is required to design and manufacture the spacecraft, placing the earliest launch date on November 1, 2026. These stringent time constraints open the possibility to use the electric thruster as main propulsion system. Indeed, even though electric propulsion systems require more complex operations, they allow wider departure and arrival windows. In addition, the amount of propellant they require is significantly lower and single-point failure effects are not as catastrophic as they would be when chemical propulsion is considered, since maneuvers are not strongly time-driven. Overall, electric propulsion is a suitable solution for a fast mission to Apophis.

The probe wet initial mass m_0 has been assumed to be 500 kg, with 73 kg of available propellant m_p . The dry mass represents more than the 85% of the total mass, corresponding to a typical value for this class of spacecraft. The selected values for the maximum-thrust-to-initial-mass ratio T_{\max}/m_0 and for the specific impulse I_{sp} for the electric propulsion subsystem are $1.2 \times 10^{-4} \text{ m/s}^2$ and 1500 s, respectively, which are compatible with state-of-the-art Hall-effect thrusters (Dannenmayer and Mazouffre, 2009). Accordingly, the maximum value for the thrust T_{\max} is 60 mN.

The spacecraft is inserted directly into an interplanetary transfer to Apophis by a launcher. Considering the characteristics of Ariane 6.2 and 6.4 launchers², the infinity velocity v_∞ at the Earth sphere-of-influence interface has been constrained to be lower than 4 km/s, with free declination δ and right ascension α in the J2000 reference frame. The analysis considers a two-body problem dynamics, with the Sun as the central body. The main assumptions for the Apophis reachability analysis are listed in Table 1.

3 Approach

The procedure followed to analyze the reachability of Apophis has to be fast and reliable, since thousands of fuel-optimal (FO) trajectories must be computed. The output of this analysis is a porkchop plot that shows the propellant mass required to reach Apophis and the reachability of the target for different departure dates and times of flight, considering the assumptions in Table 1. This assessment has the aim

²Ariane 6 User Manual I2R0: <https://www.arianespace.com/wp-content/uploads/2021/03/Mua-6-Issue-2-Revision-0-March-2021.pdf> (last accessed: July 7, 2023)

Time Constraints	Earliest departure date	November 1, 2026
	Max. Time of Flight ToF _{max}	800 days
	Latest arrival	February 13, 2029
Spacecraft	m_0	500 kg
	Propulsion	Continuous
	T_{\max}/m_0	1.2×10^{-4} m/s ²
	I_{sp}	1500 s
	T_{\max}	60 mN
	m_p	73 kg
Launcher	v_∞	≤ 4 km/s
	α	$\in [-90, +90]$ deg
	δ	$\in [-180, +180]$ deg

Table 1: Search space assumptions to perform the reachability analysis.

to evaluate the launching conditions and compute the trajectories spanning the whole temporal search space. The approach for this analysis exploits two layers:

1. A direct sequential convex programming (SCP) algorithm (Morelli et al, 2021), used for each departure date and time of flight. It gives a first assessment of the optimal launching conditions and trajectory, as it allows to easily include the free infinite velocity given by the launcher;
2. The outputs of the first step are used to feed an indirect method (Zhang et al, 2015), able to guarantee optimality of the solution in terms of propellant mass.

This two-layer approach is employed to exploit the easy handling of the free launching conditions of the first method and the guaranteed optimality of the second one. The minimum-fuel problem is solved with fixed initial and final boundary conditions, and time of flight. The initial boundary condition is variable in the first step of the methodology and fixed in the second.

3.1 Convex Optimization with Free Infinite Velocity

In the first step, the nonconvex low-thrust trajectory optimization problem is solved by considering a sequence of convex subproblems whose solutions eventually converge, under certain hypotheses, to the solution of the original one (Malyuta et al, 2022). At each iteration, the following problem is solved (Wang and Grant, 2018; Hofmann et al, 2023)

$$\underset{\mathbf{u}(t)}{\text{minimize}} \quad -w(t_f) + \lambda \max(0, \eta(t)) + \lambda \|\boldsymbol{\nu}(t)\|_1 \quad (1a)$$

$$\text{subject to:} \quad \dot{\mathbf{x}}(t) = \mathbf{f}(\bar{\mathbf{x}}(t), \bar{\mathbf{u}}(t)) + \mathbf{A}(\bar{\mathbf{x}}(t)) (\mathbf{x}(t) - \bar{\mathbf{x}}(t)) + \mathbf{B}(\mathbf{u}(t) - \bar{\mathbf{u}}(t)) + \boldsymbol{\nu}(t) \quad (1b)$$

$$\Gamma(t) \leq T_{\max} e^{-\bar{w}(t)} (1 - w(t) + \bar{w}(t)) + \eta(t) \quad (1c)$$

$$\|\boldsymbol{\tau}(t)\|_2 \leq \Gamma(t) \quad (1d)$$

$$\|\mathbf{x}(t) - \bar{\mathbf{x}}(t)\|_1 \leq R \quad (1e)$$

$$\mathbf{r}(t_i) = \mathbf{r}_i, \mathbf{v}(t_i) = \mathbf{v}_i, w(t_i) = w_i \quad (1f)$$

$$\mathbf{r}(t_f) = \mathbf{r}_f, \mathbf{v}(t_f) = \mathbf{v}_f \quad (1g)$$

$$\mathbf{x}_l \leq \mathbf{x} \leq \mathbf{x}_u, \mathbf{u}_l \leq \mathbf{u} \leq \mathbf{u}_u \quad (1h)$$

where $\mathbf{x} = [\mathbf{r}, \mathbf{v}, w]$ and $\mathbf{u} = [\tau_x, \tau_y, \tau_z, \Gamma] = [\boldsymbol{\tau}, \Gamma]$ are the state and control variables, respectively. The quantities $\eta(t)$ and $\boldsymbol{\nu}(t)$ are slack variables to avoid the so-called artificial infeasibility, and the constant parameter λ in the objective function is a user-defined weight. The times t_i and t_f are the initial and final transfer times. R is the radius of the trust region assuring that the convexification of the problem is valid. The reader can refer to previous works (Bonalli et al, 2019) for a more comprehensive explanation of the SCP technique. In Eq. (1b), the matrices \mathbf{A} and \mathbf{B} are defined as

$$\mathbf{A}(\bar{\mathbf{x}}(t)) := \left. \frac{\partial \mathbf{f}}{\partial \mathbf{x}} \right|_{\bar{\mathbf{x}}(t)}, \mathbf{B} := \left. \frac{\partial \mathbf{f}}{\partial \mathbf{u}} \right|_{\bar{\mathbf{u}}(t)} \quad (2)$$

where

$$\mathbf{f}(\mathbf{x}, \mathbf{u}) = \begin{bmatrix} \mathbf{v}(t) \\ -\frac{\mu}{r^3} \mathbf{r}(t) + \boldsymbol{\tau}(t) \\ -\frac{\Gamma(t)}{I_{sp} g_0} \end{bmatrix} \quad (3)$$

with $r = \|\mathbf{r}(t)\|_2$. The problem in Eqs. (1) is a Second-Order Cone Program (SOCP) and can be handled by efficient convex solvers. In this work, it has been solved using an Hermite–Simpson discretization scheme (Morelli et al, 2021) and the Embedded CONic Solver (ECOS) (Domahidi et al, 2013).

In order to account for the additional degree of freedom provided by the launcher, the problem is enhanced as follows:

1. Three additional variables v_∞^x, v_∞^y , and v_∞^z are introduced and collected in the vector $\mathbf{v}_\infty \in \mathbb{R}^3$.
2. The initial boundary conditions on the velocity of the spacecraft in Eq. (1f) are expressed as

$$\mathbf{v}_i = \mathbf{v}_E(t_i) + \mathbf{v}_\infty \quad (4)$$

where $\mathbf{v}_E(t_i)$ indicates the velocity of the Earth at the initial time t_i .

3. In J2000, it is possible to express the constraints on the maximum magnitude of the infinite velocity and on its maximum declination in Table 1 as

$$\|\mathbf{v}_\infty\|_2 \leq v_\infty^{\max} \quad (5a)$$

$$-v_\infty^{z, \max} \leq v_\infty^z \leq v_\infty^{z, \max} \quad (5b)$$

$$v_\infty^{z, \max} = v_\infty^{\max} \sin \tilde{\delta} \quad (5c)$$

where $\tilde{\delta}$ is the maximum allowable declination. Note that the constraint in Eq. (5a) is a Second-Order Cone Constraint (SOCC). Therefore, considering the constraints in Eqs. (5) still makes the problem in Eqs. (1) convex. It is worth to explicitly mention that the right ascension of the infinite velocity is instead free to vary.

Although the SCP algorithm is rather robust (Hofmann et al, 2023), the solution of a given problem depends on the initial guess. Therefore, to obtain an homogeneous

porkchop plot, a continuation method has been used, which considers the solutions of already-solved problems as initial guess for their neighbours. This also helps reducing significantly the computational time (Topputo et al, 2021). The continuation procedure can be summarized as follows.

1. First, the trajectory associated with the earliest departure date and longest duration is computed with a simple shape-based initial guess. This trajectory corresponds to the green box of the matrix in Fig. 1.
2. The search space is discretized using time grids. In particular, a number M of times of flight and a number N of departure dates are considered.
3. Then, for all $i = M - 1, \dots, 1$ and earliest departure date, the solution of the (already solved) problem associated with higher time of flight is interpolated to obtain the initial guess. Since an Hermite–Simpson discretization scheme is used, the state in each trajectory segment is a third-order polynomial. If the step in the time of flight direction is fairly small, the state of Apophis correspondent to the cases $i - 1$ and i is similar, and therefore the considered trajectory represents a consistently good initial guess. In the case when the optimal control problem $(i - 1, 1)$ did not converge, a cubic-based initial guess is instead used for the problem $(i, 1)$.
4. Once the trajectories associated with all the time of flights and first departure date have been computed, an additional continuation is performed. In particular, for all departure dates $j = 2, \dots, N$, the solution of the problem with time of flight i and departure date $j - 1$ is used from the new departure date j to the arrival date associated with the trajectory $(i, j - 1)$ to obtain the initial guess for the problem (i, j) . In case the case $(i, j - 1)$ did not converge, a shape-based initial guess is used instead.
5. For each of the departure dates, the FO trajectory with lower time of flight that reached convergence is finally used as initial guess to solve the time-optimal (TO) problem as well (Morelli et al, 2021). This continuation corresponds to the last separated row of the matrix in Fig. 1.

In order to further speed-up the convergence process, the number of nodes used by the algorithm to solve the problems is considered to be directly proportional to the time of flight. In particular, a number of nodes $P_{\max} = 150$ for the largest time of flight $\text{ToF}_{\max} = 800$ days is chosen, and therefore

$$P = \left\lceil P_{\max} \frac{\text{ToF}}{\text{ToF}_{\max}} \right\rceil \quad (6)$$

To properly detect the variations in propellant mass m_p and having a more efficient continuation, a variable step grid in the time-of-flight dimension is exploited. From ToF of 244 days up to 460 days, the time step has been considered to be 1 day, while a 20-day interval is considered from 460 on. This step is necessary to refine the porkchop in the zone closer to the TO solution, where both the convex and the indirect solvers benefit from denser discretization grids. Contrarily, the time step for the departure dates is fixed and set to 5 days. This grid requires about 16,000 trajectories to be computed, confirming that a fast methodology is needed to assess the feasibility of a low-thrust mission to Apophis.

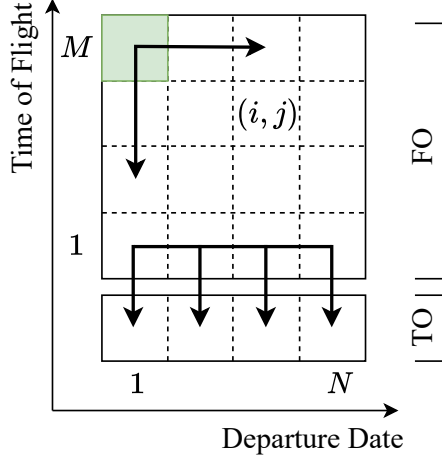


Fig. 1: Continuation scheme for the feasibility plot adopted in the two layers.

3.2 Indirect Optimization Refinement

The results obtained with the convex step are used as inputs for the indirect formulation and the generation of the final porkchop. Differently from direct methods, indirect ones aim at satisfying the necessary optimality conditions of the low-thrust trajectory optimization problem, which are derived through the calculus of variations (Kechichian, 1997). The methodology developed in previous works (Zhang et al, 2015) is used. It solves the shooting problem that stems from the imposition of the necessary conditions as specified here after. In particular, the augmented dynamical equations of states $[\mathbf{r}, \mathbf{v}, m]$ and costates $[\lambda_r, \lambda_v, \lambda_m]$ for the two-body problem are considered (Wang and Topputo, 2022)

$$\dot{\mathbf{y}} = \mathbf{F}(\mathbf{y}) \Rightarrow \begin{cases} \dot{\mathbf{r}} = \mathbf{v} \\ \dot{\mathbf{v}} = -\frac{\mu}{r^3} \mathbf{r} + u \frac{T_{max}}{m} \boldsymbol{\alpha} \\ \dot{m} = -u \frac{T_{max}}{I_{sp} g_0} \\ \dot{\lambda}_r = -\frac{3\mu}{r^5} (\mathbf{r} \cdot \lambda_v) \mathbf{r} + \frac{\mu}{r^3} \lambda_v \\ \dot{\lambda}_v = -\lambda_r \\ \dot{\lambda}_m = -u \frac{T_{max}}{m^2} \lambda_v \end{cases} \quad (7)$$

where $u(t) \in [0, 1]$ is the throttle factor and $\boldsymbol{\alpha}(t)$ is the thrust direction vector, and have to be imposed to their optimal value $\mathbf{u}^*(t) = [u^*(t), \boldsymbol{\alpha}^*(t)]$ such that the Pontryagin Maximum Principle (Bryson and Ho, 1975) is respected. To integrate these equations, the algorithm enforces the initial conditions at t_i for both the TO and FO problems

$$\mathbf{r}(t_i) - \mathbf{r}_i = \mathbf{0}, \quad \mathbf{v}(t_i) - \mathbf{v}_i = \mathbf{0}, \quad m(t_i) - m_0 = 0 \quad (8)$$

The initial mass m_0 is constant and considered equal to 500 kg as per the assumptions in Table 1, whereas \mathbf{r}_i is the initial position of the Earth, which varies with the departure date considered in each point of the search space mesh. The initial velocity is defined from the results of the convex optimization step. In particular, according to Eq. (4), it is

$$\mathbf{v}_i = \mathbf{v}_E(t_i) + \mathbf{v}_\infty = \begin{bmatrix} v_{E,x}(t_i) + v_\infty \cos \alpha \cos \delta \\ v_{E,y}(t_i) + v_\infty \sin \alpha \cos \delta \\ v_{E,z}(t_i) + v_\infty \sin \delta \end{bmatrix} \quad (9)$$

where v_∞ , α , and δ , come from the results of the first convex layer.

To obtain the solutions in the search space mesh, the same continuation scheme described in Fig. 1 is exploited for the indirect formulation. We first solve the FO problem: $\mathbf{y}(t) = \varphi(\mathbf{y}_i, t_i, t)$ being the solution flow integrated from t_i to a generic time instant t , the FO shooting problems aim to find $\boldsymbol{\lambda}_i^* = \boldsymbol{\lambda}^*(t_i)$ such that the solution at the final time t_f , namely $\mathbf{y}(t_f) = \varphi([\mathbf{x}_i, \boldsymbol{\lambda}_i^*], t_i, t_f)$, satisfies the boundary conditions

$$\begin{bmatrix} \mathbf{r}(t_f) - \mathbf{r}_f \\ \mathbf{v}(t_f) - \mathbf{v}_f \\ \lambda_m(t_f) \end{bmatrix} = \mathbf{0} \quad (10)$$

where \mathbf{r}_f and \mathbf{v}_f are the known final position and velocity of Apophis, respectively, which depend on the arrival date considered for the specific point of the search space mesh. In the integration of the flow, it can be proved (Zhang et al, 2015) that the optimal thrust vector can be expressed as $\boldsymbol{\alpha}^* = -\frac{\boldsymbol{\lambda}_v}{\lambda_v}$, whereas the optimal throttle factor u^* has the following structure:

$$u^* = \begin{cases} 0 & \text{if } S_{FO} > 0 \\ \in [0, 1] & \text{if } S_{FO} = 0 \\ 1 & \text{if } S_{FO} < 0 \end{cases} \quad (11)$$

where S_{FO} is the FO switching function, $S_{FO} = 1 - \lambda_m - \lambda_v \frac{I_{sp} g_0}{m}$. When solving the TO problem, the objective is to find the pair $[\lambda_i^*, t_f^*]$ such that $\mathbf{y}(t_f^*) = \varphi([\mathbf{x}_i, \boldsymbol{\lambda}_i^*], t_i, t_f^*)$ obtained by the integration of Eq. (7) satisfies the boundary conditions

$$\begin{bmatrix} \mathbf{r}(t_f) - \mathbf{r}_T(t_f) \\ \mathbf{v}(t_f) - \mathbf{v}_T(t_f) \\ \lambda_m(t_f) \\ H_t(t_f) - \boldsymbol{\lambda}_r(t_f) \cdot \mathbf{v}_f - \boldsymbol{\lambda}_v(t_f) \cdot \mathbf{a}_f \end{bmatrix} = \mathbf{0} \quad (12)$$

where H_t is the Hamiltonian of the TO problem, i.e., $H_t = 1 + \boldsymbol{\lambda}^T \cdot \mathbf{f}$ with $\mathbf{f} = \mathbf{f}(\mathbf{x}(t), \mathbf{u}(t))$ being the dynamics of the spacecraft, and $\mathbf{a}_f = \dot{\mathbf{v}}_f$ is the acceleration of Apophis at the final time. In the integration for the TO problem, the optimal $\boldsymbol{\alpha}^*$ and u^* follow the same logic of the FO problem, apart from the switching function which is replaced with the TO switching function $S_{TO} = -\lambda_m - \lambda_v \frac{I_{sp} g_0}{m}$. To solve the TO problem the values of v_∞ , α , and δ obtained from the convex layer are exploited, as well as the value of the ToF, which is used as initial guess for the optimal t_f^* .

4 Results

Considering the mission constraints in Table 1 and the approach in Section 3, three different analyses are carried out. First, a reachability assessment over the full departure and arrival windows is performed with a nominal thrust-to-mass ratio. Three convenient launch windows are identified and therefore three correspondent representative trajectories are analysed. Finally, it is shown that a fourth launch window can open up if engines with higher thrust-to-mass ratios are considered. Details about these analyses are provided in the remainder.

4.1 Reachability assessment

Figure 2 shows the porkchop plot related to the reachability of the Apophis asteroid under nominal conditions. This and the following plots are to be read as follows:

- The x -axis represents the departure date;
- The y -axis represents the time of flight;
- The color code represents the quantity of interest, indicated on the colorbar on the right of the plot;
- The patched red area indicates rendezvous happening after the latest arrival accordingly to Table 1, and that are therefore unfeasible;
- The oblique dashed segments represent rendezvous dates coinciding with, from up to down respectively, -3, -4, -5, and -6 months from Apophis' closest encounter with the Earth;
- The bold blue line indicates time-optimal solutions, i.e., the interplanetary transfers for which the thruster is kept on for the whole time of flight. Note that for a given departure date, solutions with lower times of flight are unfeasible (corresponding to the blue-dashed area);
- The dashed black line represents the available propellant of 73 kg.

The irregular behaviour at the center of the porkchop is related to the fly-by at the Earth. In that point, a quasi-impulsive velocity change is experienced by the asteroid in the heliocentric reference frame, making it difficult for the optimizer finding a solution for the rendezvous. Figure 3 shows the required ΔV , computed using the Tsiolkovsky equation as $\Delta V = I_{sp}g_0 \ln \frac{m_0}{m_f}$.

Results show that, under the considered hypotheses, there are three feasible launch windows, namely:

- A first one, with launch dates between November and December 2026 and times of flight that span from 540 and 800 days approximately (upper-left part of Fig. 2);
- A second one, with launch dates between April and May 2027 and times of flight of 620-660 days;
- A third one, consistently larger, with launch dates from September to November 2027, and times of flight spanning from 250 to 500 days.

Figures 4 present the optimal magnitude, declination, and right ascension, respectively, of the excess velocity of the spacecraft with respect to the Earth in the equatorial, heliocentric reference frame (J2000) as a function of the departure date and time of flight. In all the aforementioned windows, the norm of the excess velocity reaches the maximum allowable value. Moreover, the optimal declination of the excess velocity in

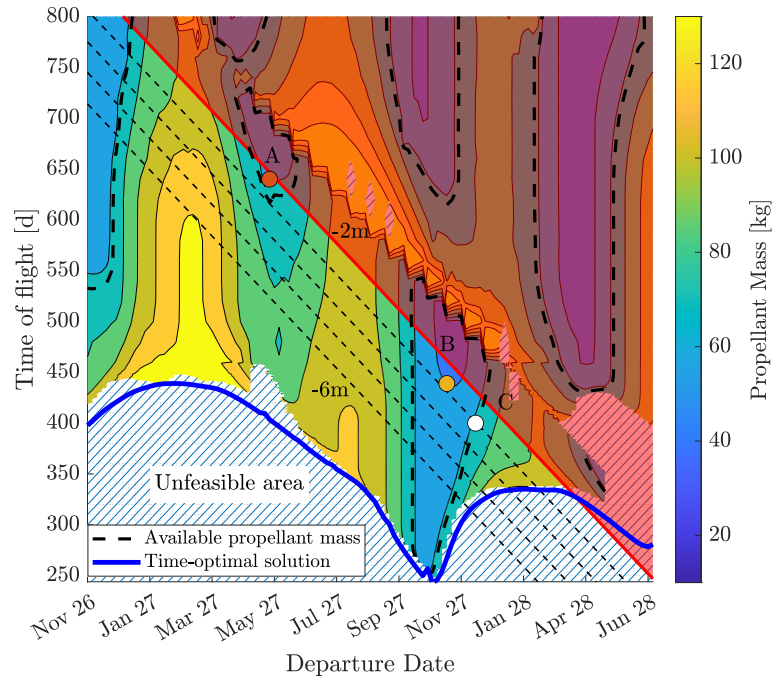


Fig. 2: Propellant mass porkchop plot.

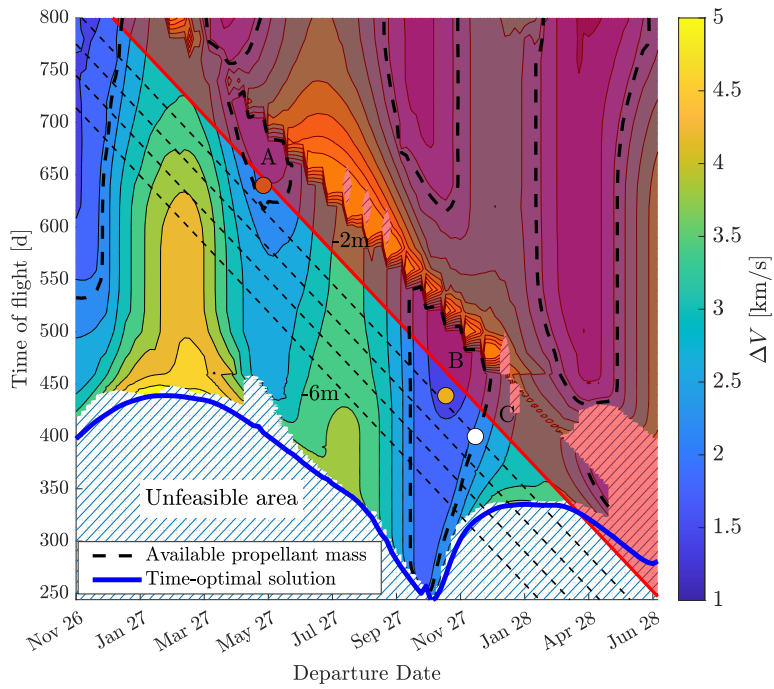
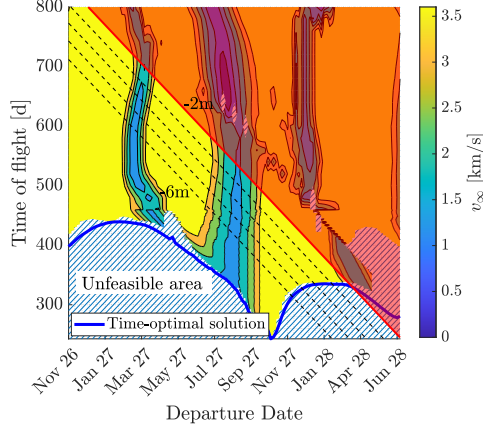
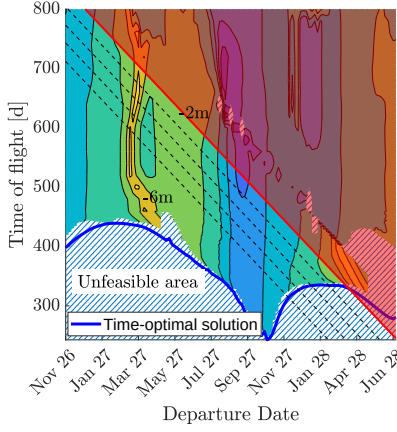


Fig. 3: ΔV porkchop plot.

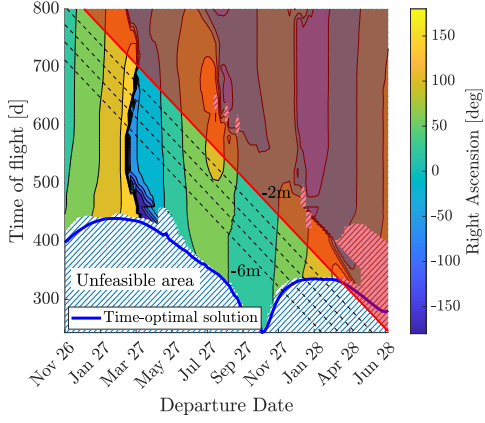
the regions of interest never assumes large values and it is included between ± 40 deg, values which are compatible with the Ariane 6.2 and 6.4 launchers.



(a) Excess velocity magnitude v_{∞} .



(b) Excess velocity declination δ .



(c) Excess velocity right ascension α .

Fig. 4: Characteristics of the optimal excess velocity provided by the launcher for each departure date and time of flight.

Figures 5 show the computational time required for the two layers of the methodology. Results refer to the first departure date. A single optimal solution requires at most 15 s to run both the layers, with a mean runtime of less than 9 s. Additionally, it is worth noting that the continuation scheme proves beneficial in expediting the identification of solutions with lower ToF. Typically, these solutions require longer computation times due to their proximity to the time-optimal solution. As a matter of fact, the convex layer requires less than 1 s to compute the optimal solution. The indirect layer requires slightly longer times due to the internal continuation from the energy- to the

fuel-optimal problem (Zhang et al, 2015). In conclusion, only few hours are required to compute the porkchop plot and complete the reachability analysis.

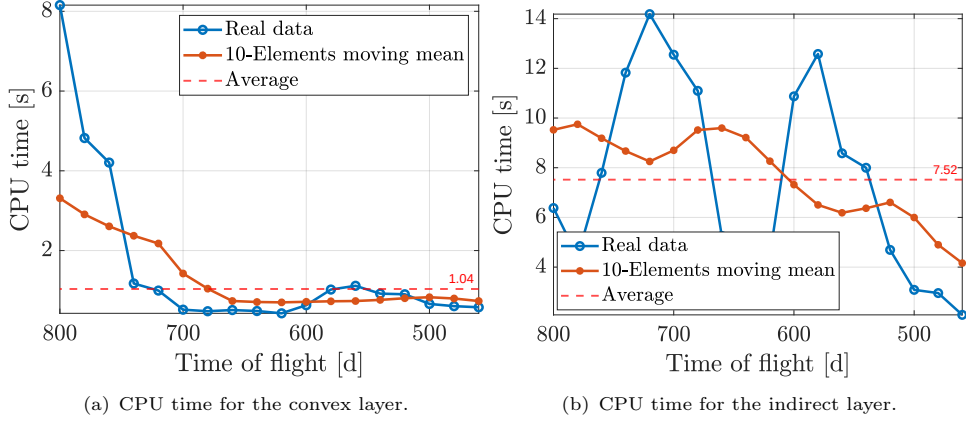


Fig. 5: CPU time required for all converged times of flight at the earliest departure date.

4.2 Candidate Trajectories

From the reachability analysis presented in Fig. 2, three sample trajectories have been selected, indicated with three dots:

- A. (dark orange dot): Departure date on May 10, 2027;
- B. (yellow dot): Departure date on November 11, 2027;
- C. (white dot): Departure date on December 11, 2027.

The three trajectories have been selected because they are respectively relevant due to A. an early launch date that would allow backup solutions in case of failure, B. a convenient required propellant mass significantly lower than the others, and C. a later launch date that would still allow an early arrival at Apophis with required propellant mass similar to the solution A. No trajectory has been selected in the first available window (i.e., between November and December 2026) as a launch in this period could be too early for the completion of the mission design phases. The characteristics of the selected trajectories have been reported in Table 2. Note that each of them requires a propellant mass value lower than 73 kg, and arrives two-to-three months before the close encounter to ensure sufficient time for pre-fly-by characterization of Apophis. The thrusting profiles of the selected trajectories are shown in Fig. 6. In Figs. 7–9 some preliminary geometrical considerations relative to the selected transfers are reported, as well as the interplanetary trajectories in the heliocentric equatorial frame.

As expected, solution A exhibits a rather empty thrust profile, while trajectory C requires longer and more frequent thrusting arcs. This behaviour correlates with the distance from the time-optimal solution. On the other hand, there is no significant differences in the distance and in the geometric quantities. This finding can simplify the

ID	Departure date	Arrival date	ToF (d)	m_p (kg)	ΔV (km/s)
A	May 10, 2027	Feb 8, 2029	640	70.43	2.21
B	Nov 11, 2027	Jan 23, 2029	439	54.95	1.69
C	Dec 11, 2027	Jan 14, 2029	400	72.23	2.29

Table 2: Characteristics of the selected representative trajectories.

system design, since communications with the ground, power generation, and relative navigation with the target are not severely affected by the trajectory of choice.

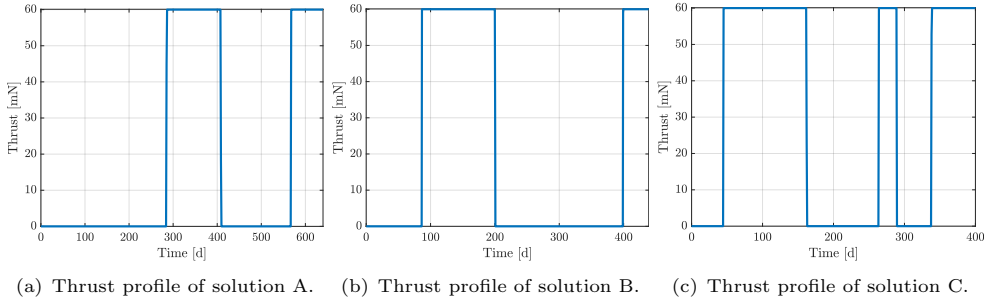


Fig. 6: Thrust profiles of trajectories A, B, and C.

4.3 Analyses with Higher Thrust-to-Mass Ratios

The nominal analysis has been conducted considering a T_{\max}/m_0 of $1.2 \times 10^{-4} \text{ m/s}^2$, corresponding to a thrust of 60 mN. In order to explore if additional opportunities are present when different propulsive systems are considered, a sensitivity analysis is performed, considering higher thrust-to-mass ratios, on the bottom right portion of Fig. 2. A possible window in this region will allow a late launch to the asteroid, giving more time for the design and integration of the spacecraft.

Figs. 10 show that an additional window that satisfies the time and propellant constraints opens up in the timespan March–May 2028 with 270–360 days of time of flight, when thrusters with slightly higher thrust-to-mass ratios are considered (namely, $1.8 \times 10^{-4} \text{ m/s}^2$ and $2 \times 10^{-4} \text{ m/s}^2$ corresponding to, respectively, thrust levels of 90 mN and 100 mN and the nominal initial mass of 500 kg). For these plots, the patched red area indicates rendezvous happening later than one month before the close encounter of the asteroid with the Earth. In conclusion, higher thrust levels may open up new feasible launch windows and thus improve the asteroid reachability.

5 Conclusion

In the context of the RAMSES mission, a fast and robust methodology has been introduced to evaluate the reachability of Apophis with a low-thrust satellite before its

close encounter with the Earth on April 13, 2029. To this aim, porckchop plots from the Earth to Apophis have been computed using a two-layer approach, exploiting a direct sequential convex programming algorithm followed by an indirect method. This method allows an easy handling of the free launching condition, while guaranteeing optimality of the solution, and it is able to compute more than 16,000 trajectories in few hours. Under the considered hypotheses, three feasible launching windows are identified. Each window lasts about 3 months and is separated from the other by about half a year, with the last one opening in September 2027. A fourth late short window, between April and May 2029, can be found if higher thrust-to-mass ratios are considered.

Acknowledgments. This work has been performed in response to ESA call AO/1-11659/23/NL/GLC: Pre-phase A/Phase A System Study of an Apophis Mission (RAMSES Definition Phase).

Conflict of interest. The authors declare that they have no known competing financial interests or personal relationships that could have appeared to influence the work reported in this paper.

References

- Binzel R, Barbee B, Barnouin O, et al (2021) Apophis 2029: Decadal opportunity for the science of planetary defense. *Bulletin of the AAS* 53(4). <https://doi.org/10.3847/25c2cfef.f87e0599>
- Bonalli R, Cauligi A, Bylard A, et al (2019) Gusto: Guaranteed sequential trajectory optimization via sequential convex programming. In: 2019 International Conference on Robotics and Automation (ICRA), pp 6741–6747, <https://doi.org/10.1109/ICRA.2019.8794205>
- Bryson A, Ho YC (1975) *Applied optimal control*. Taylor & Francis, London, <https://doi.org/10.1201/9781315137667>
- Chesley SR (2005) Potential impact detection for near-Earth asteroids: The case of 99942 Apophis (2004 MN4). *Proceedings of the International Astronomical Union* 1(S229):215–228. <https://doi.org/10.1017/S1743921305006769>
- Dannenmayer K, Mazouffre S (2009) Elementary scaling laws for the design of low and high power Hall effect thrusters. In: *Progress in Propulsion Physics, EDP Sciences*, pp 601–616
- DellaGiustina D, Golish D, Guzewich S, et al (2022) Osiris-APEX: A proposed OSIRIS-REx extended mission to Apophis. *LPI Contributions* 2681:2011
- DeMartini JV, Richardson DC, Barnouin OS, et al (2019) Using a discrete element method to investigate seismic response and spin change of 99942 Apophis during its 2029 tidal encounter with Earth. *Icarus* 328:93–103. <https://doi.org/10.1016/j.icarus.2019.03.015>

- Domahidi A, Chu E, Boyd S (2013) ECOS: An SOCP Solver for Embedded Systems. In: European Control Conference, Zurich, Switzerland, pp 3071–3076, <https://doi.org/doi:10.23919/ECC.2013.6669541>
- Giorgini JD, Benner LA, Ostro SJ, et al (2008) Predicting the Earth encounters of (99942) Apophis. *Icarus* 193(1):1–19. <https://doi.org/10.1016/j.icarus.2007.09.012>
- Hofmann C, Morelli AC, Topputo F (2023) Performance assessment of convex low-thrust trajectory optimization methods. *Journal of Spacecraft and Rockets* 60(1). <https://doi.org/10.2514/1.A35461>
- Kechichian JA (1997) Optimal low-Earth-orbit-geostationary-Earth-orbit intermediate acceleration orbit transfer. *Journal of Guidance, Control, and Dynamics* 20(4):803–811. <https://doi.org/10.2514/2.4116>
- Kim Y, DeMartini JV, Richardson DC, et al (2023) Tidal resurfacing model for (99942) Apophis during the 2029 close approach with Earth. *Monthly Notices of the Royal Astronomical Society* 520(3):3405–3415. <https://doi.org/10.1093/mnras/stad351>
- Machuca P, Sanchez JP, Masdemont JJ, et al (2020) High-fidelity trajectory design to flyby near-Earth asteroids using CubeSats. *Acta Astronautica* 167:146–163. <https://doi.org/10.1016/j.actaastro.2019.09.041>
- Malyuta D, Reynolds TP, Szmuk M, et al (2022) Convex optimization for trajectory generation: A tutorial on generating dynamically feasible trajectories reliably and efficiently. *IEEE Control Systems Magazine* 42(5):40–113. <https://doi.org/10.1109/MCS.2022.3187542>
- Morelli AC, Hofmann C, Topputo F (2021) Robust low-thrust trajectory optimization using convex programming and a homotopic approach. *IEEE Transactions on Aerospace and Electronic Systems* 58(3):2103–2116. <https://doi.org/10.1109/TAES.2021.3128869>
- Scheeres D, Benner L, Ostro S, et al (2005) Abrupt alteration of Asteroid 2004 MN4’s spin state during its 2029 Earth flyby. *Icarus* 178(1):281–283. <https://doi.org/10.1016/j.icarus.2005.06.002>
- Sokolov L, Bashakov A, Borisova T, et al (2012) Impact trajectories of the asteroid apophis in the 21st century. *Solar System Research* 46:291–300. <https://doi.org/10.1134/S0038094612040077>
- Souchay J, Souami D, Lhotka C, et al (2014) Rotational changes of the asteroid 99942 Apophis during the 2029 close encounter with Earth. *Astronomy & Astrophysics* 563:A24. <https://doi.org/10.1051/0004-6361/201322364>
- Topputo F, Wang Y, Giordano C, et al (2021) Envelop of reachable asteroids by M-ARGO CubeSat. *Advances in Space Research* 67(12):4193–4221. <https://doi.org/>

[10.1016/j.asr.2021.02.031](https://doi.org/10.1016/j.asr.2021.02.031)

- Valvano G, Winter OC, Sfair R, et al (2022) Apophis-effects of the 2029 Earth's encounter on the surface and nearby dynamics. *Monthly Notices of the Royal Astronomical Society* 510(1):95–109. <https://doi.org/10.1093/mnras/stab3299>
- Wagner S, Wie B, Barbee BW (2015) Target selection for a hypervelocity asteroid intercept vehicle flight validation mission. *Acta Astronautica* 107:247–261. <https://doi.org/10.1016/j.actaastro.2014.11.037>
- Wang Y, Topputo F (2022) Indirect optimization of power-limited asteroid rendezvous trajectories. *Journal of Guidance, Control, and Dynamics* 45(5):962–971. <https://doi.org/10.2514/1.G006179>
- Wang Z, Grant MJ (2018) Minimum-Fuel Low-Thrust Transfers for Spacecraft: A Convex Approach. *IEEE Transactions on Aerospace and Electronic Systems* 54(5):2274–2290. <https://doi.org/10.1109/TAES.2018.2812558>
- Yu Y, Richardson DC, Michel P, et al (2014) Numerical predictions of surface effects during the 2029 close approach of asteroid 99942 Apophis. *Icarus* 242:82–96. <https://doi.org/10.1016/j.icarus.2014.07.027>
- Zhang C, Topputo F, Bernelli-Zazzera F, et al (2015) Low-thrust minimum-fuel optimization in the circular restricted three-body problem. *Journal of Guidance, Control, and Dynamics* 38(8):1501–1510. <https://doi.org/10.2514/1.G001080>
- Zhang Y, Michel P (2020) Tidal distortion and disruption of rubble-pile bodies revisited-soft-sphere discrete element analyses. *Astronomy & Astrophysics* 640:A102. <https://doi.org/10.1051/0004-6361/202037856>

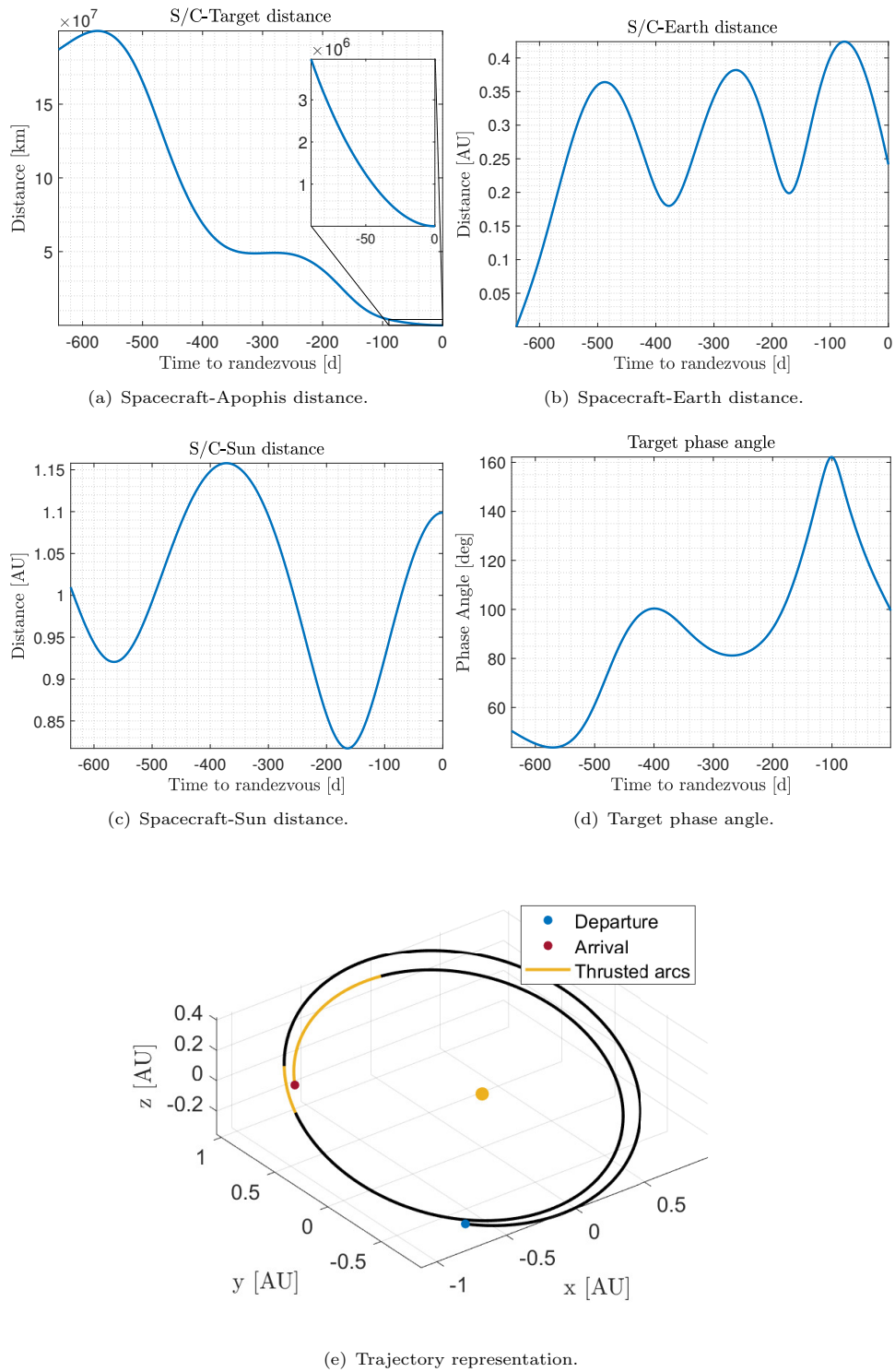


Fig. 7: Geometrical analysis and representation in the J2000 reference frame of the solution A.

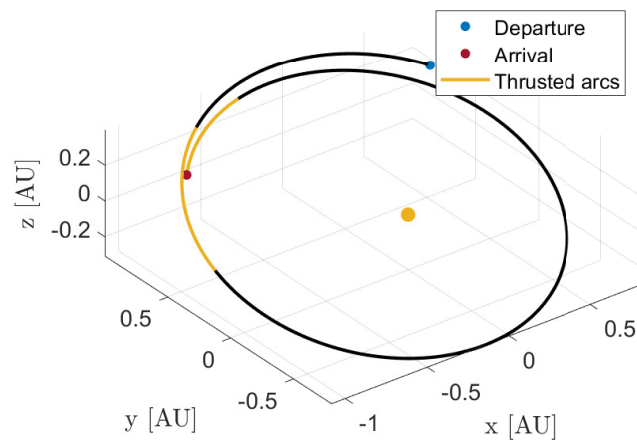
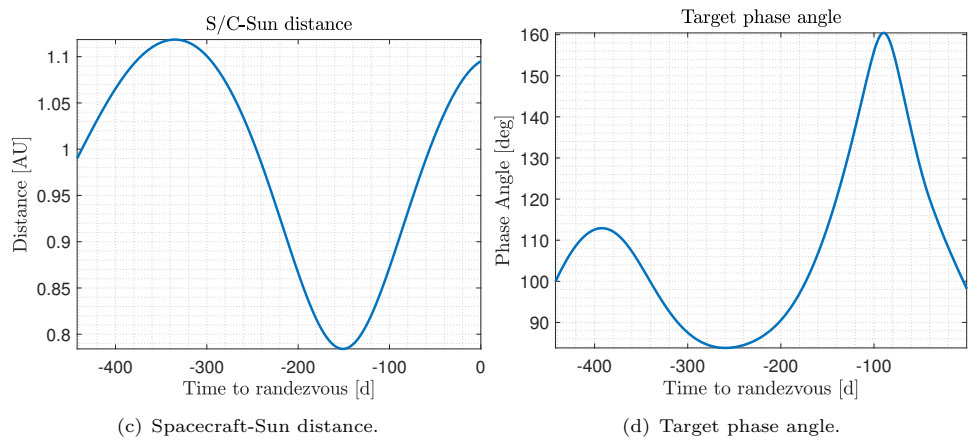
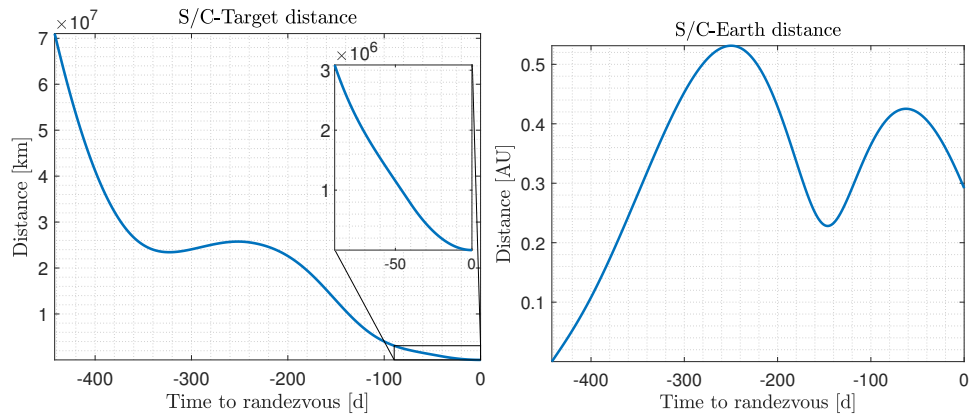


Fig. 8: Geometrical analysis and representation in the J2000 reference frame of the solution B.

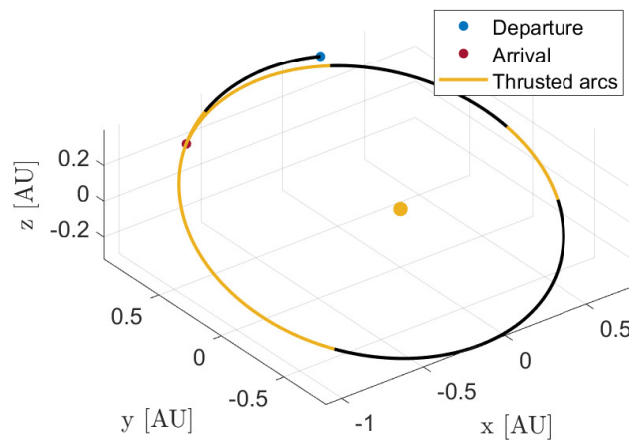
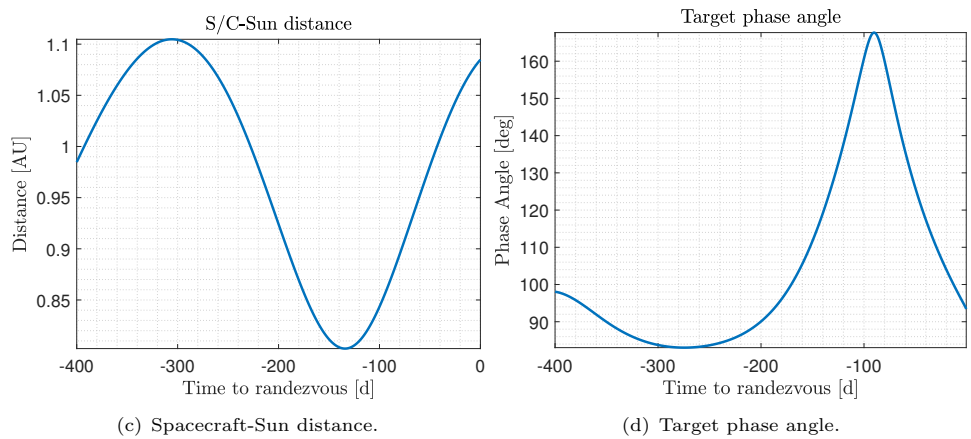
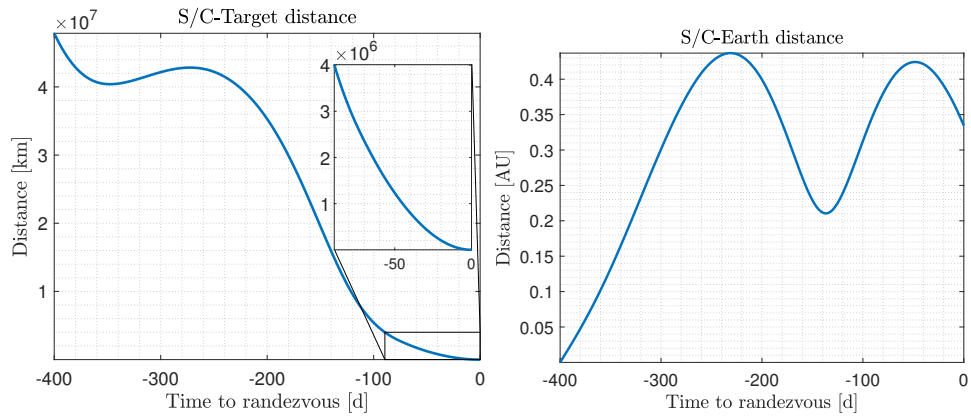


Fig. 9: Geometrical analysis and representation in the J2000 reference frame of the solution C.

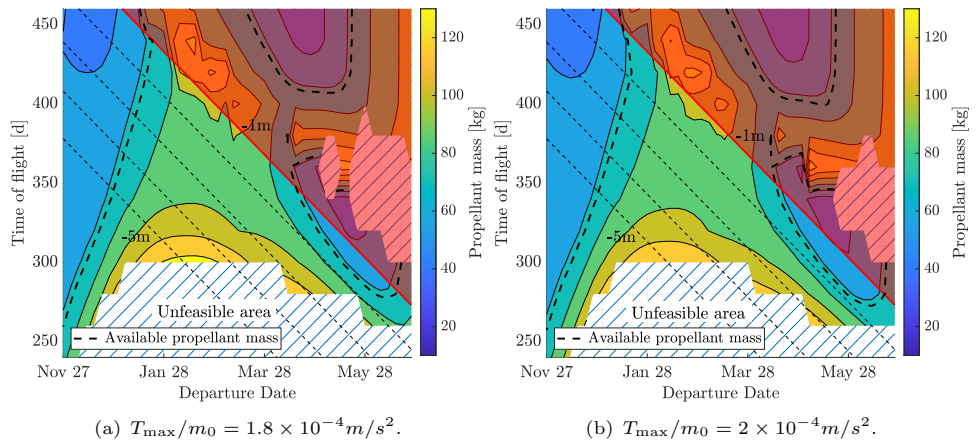


Fig. 10: Porkchop plots for higher thrust-to-mass ratios.